Published in final edited form as:
J Biomech. 2012 February 23; 45(4): 647–652. doi:10.1016/j.jbiomech.2011.12.015.

ACTIVATION AND APONEUROSIS MORPHOLOGY AFFECT IN VIVO MUSCLE TISSUE STRAINS NEAR THE MYOTENDINOUS JUNCTION

Niccolo M. Fiorentino[1], **Frederick H. Epstein**[2,3], and **Silvia S. Blemker**[1,2,4]

[1]Department of Mechanical & Aerospace Engineering, University of Virginia, Charlottesville, VA, USA

[2]Department of Biomedical Engineering, University of Virginia, Charlottesville, VA, USA

[3]Department of Radiology, University of Virginia, Charlottesville, VA, USA

[4]Department of Orthopaedic Surgery, University of Virginia, Charlottesville, VA, USA

Abstract

Hamstring strain injury is one of the most common injuries in athletes, particularly for sports that involve high speed running. The aims of this study were to determine whether muscle activation and internal morphology influence *in vivo* muscle behavior and strain injury susceptibility. We measured tissue displacement and strains in the hamstring muscle injured most often, the biceps femoris long head muscle (BFLH), using cine DENSE dynamic magnetic resonance imaging. Strain measurements were used to test whether strain magnitudes are (i) larger during active lengthening than during passive lengthening and (ii) larger for subjects with a relatively narrow proximal aponeurosis than a wide proximal aponeurosis. Displacement color maps showed higher tissue displacement with increasing lateral distance from the proximal aponeurosis for both active lengthening and passive lengthening, and higher tissue displacement for active lengthening than passive lengthening. First principal strain magnitudes were averaged in a 1 cm region near the myotendinous junction, where injury is most frequently observed. It was found that strains are significantly larger during active lengthening (0.19 SD 0.09) than passive lengthening (0.13 SD 0.06) ($p < 0.05$), which suggests that elevated localized strains may be a mechanism for increased injury risk during active as opposed to passive lengthening. First principal strains were higher for subjects with a relatively narrow aponeurosis width (0.26 SD 0.15) than wide (0.14 SD 0.04) ($p < 0.05$). This result suggests that athletes who have BFLH muscles with narrow proximal aponeuroses may have an increased risk for BFLH strain injuries.

Keywords

acute strain injury; muscle; dynamic magnetic resonance imaging; *in vivo* measurement; active lengthening

Address Correspondence: Silvia Blemker, PhD, Department of Mechanical & Aerospace Engineering, University of Virginia, 122 Engineer's Way, Charlottesville, VA 22904, Phone: 4349246291, Fax: 4349822037, ssblemker@virginia.edu.

Conflict of interest statement

We would like to declare that we do not have any conflict of interest to report in this research.

1. INTRODUCTION

Hamstring strain injury is one of the most common injuries in athletes (Clanton and Coupe, 1998), especially for sports that involve running and sprinting, such as track and field (Bennell and Crossley, 1996), soccer (Ekstrand et al., 2011), Rugby Union (Brooks et al., 2005), Australian Rules Football (Orchard and Seward, 2002), and American Football (Feeley et al., 2008). Of the three biarticular hamstring muscles, the biceps femoris long head (BFLH) muscle is injured most often (De Smet and Best, 2000; Koulouris and Connell, 2003; Verrall et al., 2003). Despite the established prevalence of acute hamstring strain injury in sport, the factors contributing to the high incidence of injury remain poorly understood (Hoskins and Pollard, 2005).

Animal muscle experiments of injury have found that muscles are most susceptible to injury when they are active and lengthening (Garrett et al., 1987; Lieber et al., 1991). These experiments have been performed at the whole-muscle level and have demonstrated that the magnitude of strain during active lengthening is the best predictor of injury (Lieber and Friden, 1993), though for passive lengthening, the strains that lead to injury are much higher than those for active lengthening (Brooks et al., 1995). However, experiments at the myofibril level found that myofibrils fail at similar sarcomere strains for both active and passive lengthening conditions (Leonard and Herzog, 2010). These two results are inconsistent from the perspective of muscle-tendon unit dynamics. One would expect fibers to stretch less during active lengthening as compared to passive lengthening, due to the fact that tendons stretch relatively more during active lengthening (Hoang et al., 2007; Zajac, 1989). If fibers stretch less during active than passive lengthening, why are muscles more susceptible to injury during active lengthening? One possible explanation is that, despite the fact that whole muscle-fiber strains may be lower during active lengthening, localized muscle tissue strains (i.e., strains in a small region of the muscle) may be higher during active lengthening as opposed to passive lengthening. However, this comparison has not been made *in vivo*.

The BFLH muscle has a bipennate structure with a narrow, cord-like proximal aponeurosis on the medial side of the muscle and a broad, thin distal aponeurosis on the lateral side (Woodley and Mercer, 2005). Recently, results from a three-dimensional model of the BFLH indicated that the BFLH's internal morphology could contribute to the muscle's increased strain injury risk (Rehorn and Blemker, 2010). The model suggested that the increased strain near the proximal myotendinous junction (MTJ) in the BFLH is due to the fact that the proximal aponeurosis is much narrower than the distal aponeurosis in this muscle and that the relative aponeurosis dimensions may be a predictor of increased strain injury susceptibility in the BFLH. However, the variability of aponeurosis width across individuals and the effect of this variability on measured strain *in vivo* have yet to be explored experimentally.

The goals of this work were to utilize cine DENSE magnetic resonance (MR) imaging to: *i)* measure tissue strains in the BFLH muscle during active lengthening and passive lengthening, *ii)* compare strain magnitudes during active lengthening and during passive lengthening in the region adjacent to the proximal aponeurosis, which is where injury is often observed (Askling et al., 2007; Silder et al., 2008), and *iii)* compare strain magnitudes in the region adjacent to the proximal aponeurosis for subjects with a relatively narrow proximal aponeurosis to those with a wide aponeurosis during active lengthening. We hypothesize that active lengthening will result in larger strain magnitudes than passive lengthening and that muscles with a narrow proximal aponeurosis will experience larger strains than those with a wide proximal aponeurosis.

2. METHODS

Subjects

Thirteen (N = 13, 5 female, 8 male) healthy subjects (mean age: 25 SD 5 years, height: 175 SD 7 cm) provided informed consent and were scanned in accordance with the University of Virginia's Institutional Review Board guidelines. All subjects had no known previous hamstring strain injury and were free from lower extremity joint pain at the time of scanning.

Experimental setup

Subjects were positioned in the headfirst, prone position on a non-ferrous exercise device (Silder et al., 2009) in a Siemens Trio 3T MR scanner (Erlangen, Germany) (Fig. 1A). Subjects performed knee flexion-extension motions at a rate of 0.5 Hz and guided by an auditory metronome. Range of motion inside the scanner depended on the leg length of the subject and was generally 30–40°. A fiber optic angular encoder (Model MR318, Microner Inc., Newbury Park, CA, USA) was fixed to an axis on the back of the device to track rotational motion during scanning (Fig. 1B). The angular encoder's optical signal was converted to a quadrature signal with a remote encoder interface (Model MR310, Microner Inc., Newbury Park, CA, USA) such that it could be read by an encoder data acquisition device (Model USB1, USDigital, Vancouver, Washington, USA) and exported to LabVIEW (National Instruments, Austin, TX, USA). A LabVIEW program analyzed the angular encoder signal to determine when maximum knee flexion had been reached and the onset of knee extension (Fig. 1C), at which time a data acquisition device (Model USB-6211, National Instruments, Austin, TX, USA) sent a square-wave pulse to the scanner to initiate image acquisition.

Static images

Axial plane images were acquired of the right thigh from the biceps femoris' origin on the ischial tuberosity to its insertion on the fibular head. Three coils were used to acquire static images—a body matrix coil on the hip, a large flex coil wrapped around the posterior thigh, and a body matrix coil on the knee. The body matrix coil on the knee was removed prior to dynamic imaging. Static images were acquired with a turbo spin echo sequence and the following parameters: field-of-view 250 × 250 mm^2, imaging matrix 512 × 512, in-plane resolution 0.49 × 0.49 mm^2, slice thickness 5 mm, TE 29 ms, TR 6000 ms and flip angle 120°. Static images were used to define the dynamic imaging plane such that it passed through the proximal aponeurosis, muscle belly and distal aponeurosis (Fig. 2A). An additional image was acquired in the dynamic imaging plane to confirm the BFLH's orientation in the imaging plane and the presence of the proximal and distal aponeuroses (Fig. 2B).

Aponeurosis width measurement

Aponeurosis width measurements were taken directly on static images using Mimics software (The Materialise Group, Leuven, Belgium). For each subject, the end of the proximal aponeurosis was identified by inspection of axial-plane images. The image that was one slice superior from the end of the aponeurosis was used for measurement. This was a more reliable measurement location than the actual end of the aponeurosis, which potentially suffers from averaging over the thickness of the imaging slice. This location was chosen for measurement location because this is precisely where strain magnitudes were found to be the largest in previous computational model simulations (Rehorn and Blemker, 2010). A width measurement was acquired by determining the length of a line drawn directly on the proximal aponeurosis (Fig. 2C). Subjects were divided into two groups based

on the median aponeurosis width, with subjects above the median placed in the wide aponeurosis group (N = 6) and those at or below the median into the narrow aponeurosis group (N = 7). The observer responsible for performing aponeurosis width measurements was blinded to the strain results and vice versa.

Dynamic imaging protocol

Cine Displacement ENcoding with Stimulated Echoes (DENSE) images were acquired in an oblique-coronal imaging plane in the BFLH muscle of the right thigh during repeated knee flexion-extension (Aletras et al., 1999; Kim et al., 2004). In a previous study of skeletal muscle motion in the biceps muscle in the arm (Zhong et al., 2008), DENSE was shown to provide strain measurements that are consistent with strains measured using cine-PC imaging (Pappas et al., 2002). DENSE images provide a measure of displacement at a pixel-wise resolution by encoding displacement directly into the phase of the MR signal (Fig. 3A). A spiral *k*-space acquisition and three-point balanced displacement-encoding technique were employed for fast data acquisition and to ensure equivalent phase noise in all directions as well as increased phase signal-to-noise (Zhong et al., 2009). Imaging parameters for the DENSE acquisition included 400 × 400 mm^2 field-of-view, 128 × 128 acquisition matrix, 8 mm slice thickness, 0.08 cycles/mm in-plane and 0.12 cycles/mm through-plane displacement-encoding frequency, TE 1.08 ms, TR 25 ms, flip angle 20°, 1800 ms acquisition window, 35 time frames, and 2.5 minutes scan time.

For active lengthening trials, rotation of inertial disks attached to the back of the device (Fig. 1B) resulted in active lengthening of the hamstring muscles (Silder et al., 2009). For passive lengthening trials, an individual standing outside the MR scanner moved the subject's leg while the subject remained relaxed. To test strain measurement repeatability, a second active lengthening or passive lengthening trial was acquired for each subject. Repeatability scans found first principal strain measurements to differ by an average of 0.06 (SD 0.03) across all subjects. In addition, an axial-plane data set was acquired in a plane near the inferior end of the proximal aponeurosis to study differences in displacement between the narrow and wide aponeurosis subjects. The order for the four trials (active lengthening, passive lengthening, repeatability, and axial-plane motion) was randomized between subjects and time for rest was included between all trials.

Displacement reconstruction and strain analysis

Time-varying tissue positions were reconstructed from DENSE images, and Lagrangian strain tensors were calculated on a pixel-wise basis (Spottiswoode et al., 2007) (Fig. 3). The BFLH muscle was outlined on DENSE images, and the MR signal's phase was converted to displacement (displacement = phase / (2π k_e), k_e = encoding frequency) at each pixel. At each time frame, *gridfit*, a function that is freely available on MATLAB's (The Mathworks, Inc., Natick, MA, USA) File Exchange, was used to spatially smooth displacements by employing a linear surface approximation over the entire BFLH region of interest. Displacement measurements at each time frame were projected back to the first time frame, and linear interpolation of the closest 3 pixels' locations was used to define a material description of tissue position at later time frames. Maximum knee flexion served as the reference configuration for zero displacement and strain calculations. Time-varying tissue positions were determined by temporal fitting with a polynomial. Data sets with a ratio of average through-plane displacement to in-plane displacement greater than 0.3 were disregarded prior to strain analysis, which included five data sets for the passive lengthening acquisitions and no acquisitions for active lengthening. The 0.3 threshold was chosen to ensure that muscle tissue remained in the imaging plane throughout the motion.

Lagrangian strain tensors were found at each pixel with the most positive eigenvalue defined as first principal strain. First principal strain values were averaged in the 1 cm region nearest the BFLH's proximal aponeurosis (i.e. near the myotendinous junction), because recent dynamic MR experiments (Silder et al., 2010) and computational models (Rehorn and Blemker, 2010) of active lengthening found that tissue strains are higher in the region adjacent to the proximal aponeurosis and this is where injury is typically observed (Askling et al., 2007; Silder et al., 2008). Statistical comparisons were made at the time frame corresponding to full extension, because injury has been observed during the terminal swing phase of sprinting gait (Heiderscheit et al., 2005; Schache et al., 2009).

A one-tailed, paired t-test was used to test whether displacements and strains were larger during active lengthening than during passive lengthening, and a one-tailed, two-sample t-test was used to test whether strains were larger for subjects with a narrow proximal aponeurosis than for subjects with a wide aponeurosis during active lengthening.

3. RESULTS

Muscle tissue displacement in the 1 cm region adjacent to the proximal aponeurosis was larger during active lengthening (9.70 SD 0.28 mm) compared to passive lengthening (6.19 SD 0.18 mm) ($p < 0.05$), which demonstrates greater stretch of the proximal tendon during active lengthening. Average 1^{st} principal strain in the 1 cm region nearest the proximal aponeurosis border (Fig. 4) was greater during active lengthening (0.19 SD 0.09) than during passive lengthening (0.13 SD 0.06) ($p < 0.05$).

Proximal aponeurosis width varied from 3.1 mm to 9.2 mm and on average was 5.8 (SD 1.8) mm for all subjects, 4.4 (SD 0.7) mm for the narrow group, and 7.3 (SD 1.3) mm for the wide group. Axial plane color maps of displacement demonstrate that displacement is smallest along the proximal aponeurosis and increases with distance from the aponeurosis (Fig. 5). In addition, color maps of displacement showed that the region of low displacement near the proximal aponeurosis had a smaller area for subjects with a narrow proximal aponeurosis as compared to subjects with a wide aponeurosis. During active lengthening, subjects with a narrow proximal aponeurosis experienced greater 1^{st} principal strain (0.26 SD 0.15) in the 1 cm region adjacent to the aponeurosis (Fig. 6) as compared to the wide aponeurosis group (0.14 SD 0.04) ($p < 0.05$).

4. DISCUSSION

This study measured *in vivo* localized strains in the BFLH muscle during active and passive lengthening conditions to answer two questions. Are localized tissue strains elevated during active as opposed to passive lengthening? And, do subjects with a narrower proximal aponeurosis demonstrate elevated localized tissue strains as compared to subjects with a wider proximal aponeurosis? We found that localized tissue strains near the proximal aponeurosis were indeed higher during active lengthening as compared to passive lengthening (Fig. 4). Furthermore, subjects with a narrower proximal aponeurosis experienced larger localized tissue strains during active lengthening than the subjects with a wider aponeurosis (Fig. 6).

Our result that *in vivo* localized muscle tissue strains are elevated during active lengthening provides an explanation for why muscles are more susceptible to injury during active lengthening conditions, as compared to passive lengthening. Previous animal models of muscle injury have shown that, while strain magnitude is an excellent predictor of injury for active lengthening (Lieber and Friden, 1993), the relationship between strain magnitude and injury potential is different between active and passive lengthening conditions (Brooks et al., 1995). By contrast, myofibril-level experiments demonstrated that the relationship between

sarcomere strain magnitude and myofibril failure is similar for both active and passive lengthening conditions (Leonard and Herzog, 2010). One possible explanation for these disparate findings is that in the animal whole muscle-tendon-unit experiments strains experienced by the muscle tissue (and sarcomeres) are different in the active as compared to the passive lengthening experiments. However, one would expect that, with the presence of a tendon, muscle fiber strains would be less during active lengthening due to increased tendon stretch in active lengthening as compared to the passive lengthening. (Our displacement results also confirm increased stretch of the proximal tendon in the active case.) Nonetheless, while overall fiber strains might be lower during active lengthening in the presence of a tendon, we found that the localized muscle tissue strains adjacent to the proximal aponeurosis were higher, which would result in increased injury potential, particularly in those regions where tissue strains are elevated. More *in vivo* studies that explore a large range of activation levels are needed in order to determine the exact relationship between activation and localized strains.

Displacement and 1st principal strain measurements were found to differ based on the BFLH's proximal aponeurosis width at the inferior end of the muscle. Example displacement color maps in an axial imaging plane (Fig. 5) showed that subjects with a narrower proximal aponeurosis width had a smaller region of low displacement adjacent to the aponeurosis (Fig. 5B); whereas subjects with a wider proximal aponeurosis had a wider, more diffuse region of low displacement near the proximal aponeurosis (Fig. 5D). Average 1st principal strains were found to be higher for subjects with a narrow proximal aponeurosis than for subjects with a wide aponeurosis (Fig. 6), suggesting that proximal aponeurosis width could influence an individual's susceptibility to strain injury by leading to increased strains in the region where injury is often observed. This result is consistent with previous modeling work that showed that the increased strain near the proximal MTJ in the BFLH is due to the fact that the proximal aponeurosis is much narrower than the distal aponeurosis in this muscle and that the relative aponeurosis dimensions may be a predictor of increased strain injury susceptibility in the BFLH (Rehorn and Blemker, 2010). In contrast, the other two hamstring muscles, which are injured less often than the BFLH (Koulouris and Connell, 2003), have a wide aponeurosis at each end of the muscle (Woodley and Mercer, 2005).

Cine DENSE imaging was performed in a single oblique-coronal imaging plane passing through the proximal aponeurosis, muscle belly, and distal aponeurosis, with the goal of capturing the mechanics of muscle tissue adjacent to the proximal aponeurosis. While this plane allowed us to accurately measure the motion of the muscle in this proximal region, it did not allow us to consistently capture the motion of the distal region of the muscle. In addition, excessive through-plane motion necessitated the removal of passive data sets for five subjects to avoid spurious in-plane strain results, which limited our ability to test for interactions between activation and aponeurosis morphology. In future studies, a larger cohort of subjects, along with additional loading conditions, will allow for a more detailed analysis of the effects of activation level and morphology on *in vivo* localized strains in the BFLH. It is also possible that extending the dynamic imaging and strain analysis to three dimensions would yield a more robust description of tissue mechanics of the whole muscle, though three-dimensional DENSE imaging over a large field-of-view requires a significant increase in scan time (e.g., 20 minutes to cover 350 × 350 × 110 mm^3 in (Zhong et al., 2010)).

The aponeurosis width measurement used in this study was taken on a single static MR image and toward the inferior end of the proximal aponeurosis. The inferior end of the proximal aponeurosis was chosen for measurement location because previous imaging studies found injury to often occur along the proximal MTJ (Askling et al., 2007; Silder et al., 2008) and computational model simulations of active lengthening predicted strain

magnitudes to be largest in this region (Rehorn and Blemker, 2010). Given the large variability in strains in the narrow aponeurosis width group, a more detailed description of aponeurosis dimensions may provide additional insights into the link between BFLH architecture and the muscle's strain injury susceptibility. For example, we noticed that some subjects exhibited a very thin curve-shaped extension of the proximal aponeurosis (a "hook") that penetrated the belly of the muscle, which could potentially influence strain distributions in this region. In addition, the local fiber arrangement in this region could be an important factor, which could be determined with diffusion tensor imaging (Englund et al., 2011). The results presented here motivate the need to conduct future studies that additionally measure other morphologic factors (such as the "hook" and the fiber arrangement) in a larger cohort of subjects to fully determine relationship between internal muscle-tendon morphology and strains.

Future prospective studies are required to confirm the extent to which the BFLH muscle's architecture contributes to acute strain injury. Muscle architectural measurements can then be integrated with risk factors that have shown promise as predictors of strain injury, because strain injury risk is likely a confluence of factors—functional and non-functional—instead of a single, stand-alone cause (Bahr and Holme, 2003). Identifying individual athletes and teams at-risk for acute strain injury can be used to motivate training programs that have demonstrated success in preventing injury and re-injury, such as eccentric strength training (Arnason et al., 2008; Askling et al., 2003) and trunk stabilization exercises (Sherry and Best, 2004).

Acknowledgments

The authors wish to acknowledge the contributions of Darryl Thelen, Amy Silder, Christopher Westphal, Michael Rehorn, Geoff Handsfield, Xiadong Zhong and Drew Gilliam. The funding for this work was provided by NIH R01 AR056201, NIH R01 EB001763 and the National Science Foundation Graduate Research Fellowship Program.

References

Aletras AH, Ding SJ, Balaban RS, Wen H. DENSE: Displacement encoding with stimulated echoes in cardiac functional MRI. Journal of Magnetic Resonance. 1999; 137:247–252. [PubMed: 10053155]

Arnason AA, Andersen TE, Holme I, Engebretsen L, Bahr R. Prevention of hamstring strains in elite soccer: an intervention study Prevention of hamstring strains in soccer. Scandinavian Journal of Medicine & Science in Sports. 2008; 18:40–48. [PubMed: 17355322]

Askling C, Karlsson J, Thorstensson A. Hamstring injury occurrence in elite soccer players after preseason strength training with eccentric overload. Scandinavian Journal of Medicine & Science in Sports. 2003; 13:244–250. [PubMed: 12859607]

Askling CM, Tengvar M, Saartok T, Thorstensson A. Acute First-Time Hamstring Strains During High-Speed Running: A Longitudinal Study Including Clinical and Magnetic Resonance Imaging Findings. The American Journal of Sports Medicine. 2007; 35:197–206. [PubMed: 17170160]

Bahr R, Holme I. Risk factors for sports injuries -- a methodological approach. British Journal of Sports Medicine. 2003; 37:384–392. [PubMed: 14514527]

Bennell KL, Crossley K. Musculoskeletal injuries in track and field: incidence, distribution and risk factors. Australian Journal of Science and Medicine in Sport. 1996; 28:69–75. [PubMed: 8937661]

Brooks JHM, Fuller CW, Kemp SPT, Reddin DB. Epidemiology of injuries in English professional rugby union: part 1 match injuries. British Journal of Sports Medicine. 2005; 39:757–766. [PubMed: 16183774]

Brooks SV, Zerba E, Faulkner JA. Injury to Muscle-Fibers After Single Stretches of Passive and Maximally Stimulated Muscles in Mice. Journal of Physiology-London. 1995; 488:459–469.

Clanton TO, Coupe KJ. Hamstring strains in athletes: diagnosis and treatment. Journal of the American Academy of Orthopaedic Surgeons. 1998; 6:237–248. [PubMed: 9682086]

De Smet AA, Best TM. MR imaging of the distribution and location of acute hamstring injuries in athletes. American Journal of Roentgenology. 2000; 174:393–399. [PubMed: 10658712]

Ekstrand J, Hagglunc M, Walden M. Epidemiology of Muscle Injuries in Professional Football (Soccer). The American Journal of Sports Medicine. 2011; 39:1226–1232. [PubMed: 21335353]

Englund EK, Elder CP, Xu Q, Ding Z, Damon BM. Combined Diffusion and Strain Tensor MRI Reveals a Heterogeneous, Planar Pattern of Strain Development during Isometric Muscle Contraction. American Journal of Physiology Regulatory, Integrative and Comparative Physiology. 2011

Feeley BT, Kennelly S, Barnes RP, Muller MS, Kelly BT, Rodeo SA, Warren RF. Epidemiology of National Football League Training Camp Injuries From 1998 to 2007. The American Journal of Sports Medicine. 2008; 36:1597–1603. [PubMed: 18443276]

Garrett WE, Safran MR, Seaber AV, Glisson RR, Ribbeck BM. Biomechanical comparison of stimulated and nonstimulated skeletal muscle pulled to failure. American Journal of Sports Medicine. 1987; 15:448–454. [PubMed: 3674268]

Heiderscheit BC, Hoerth DM, Chumanov ES, Swanson SC, Thelen BJ, Thelen DG. Identifying the time of occurrence of a hamstring strain injury during treadmill running: a case study. Clinical Biomechanics. 2005; 20:1072–1078. [PubMed: 16137810]

Hoang PD, Herbert RD, Todd G, Gorman RB, Gandevia SC. Passive mechanical properties of human gastrocnemius muscle-tendon units, muscle fascicles and tendons in vivo. Journal of Experimental Biology. 2007; 210:4159–4168. [PubMed: 18025015]

Hoskins W, Pollard H. The management of hamstring injury--Part 1: Issues in diagnosis. Manual Therapy. 2005; 10:96–107. [PubMed: 15922230]

Kim D, Gilson WD, Kramer CM, Epstein FH. Myocardial Tissue Tracking with Two-dimensional Cine Displacement-encoded MR Imaging: Development and Initial Evaluation. Radiology. 2004; 230:862–871. [PubMed: 14739307]

Koulouris G, Connell D. Evaluation of the hamstring muscle complex following acute injury. Skeletal Radiology. 2003; 32:582–589. [PubMed: 12942206]

Leonard TR, Herzog W. Regulation of muscle force in the absence of actin-myosin-based cross-bridge interaction. American Journal of Physiology-Cell Physiology. 2010; 43:3063–3066.

Lieber RL, Friden J. Muscle damage is not a function of muscle force but active muscle strain. Journal of Applied Physiology. 1993; 74:520–526. [PubMed: 8458765]

Lieber RL, Woodburn TM, Friden J. Muscle damage induced by eccentric contractions of 25% strain. Journal of Applied Physiology. 1991; 70:2498–2507. [PubMed: 1885443]

Orchard J, Seward H. Epidemiology of injuries in the Australian Football League, seasons 1997–2000. British Journal of Sports Medicine. 2002; 36:39–45. [PubMed: 11867491]

Pappas GP, Asakawa DS, Delp SL, Zajac FE, Drace JE. Nonuniform shortening in the biceps brachii during elbow flexion. Journal of Applied Physiology. 2002; 92:2381–2389. [PubMed: 12015351]

Rehorn MR, Blemker SS. The effects of aponeurosis geometry on strain injury susceptibility explored with a 3D muscle model. Journal of Biomechanics. 2010; 43:2574–2581. [PubMed: 20541207]

Schache AG, Wrigley TV, Baker R, Pandy MG. Biomechanical response to hamstring muscle strain injury. Gait & Posture. 2009; 29:332–338. [PubMed: 19038549]

Sherry MA, Best TM. A comparison of 2 rehabilitation programs in the treatment of acute hamstring strains. Journal of Orthopaedic & Sports Physical Therapy. 2004; 34:116–125. [PubMed: 15089024]

Silder A, Heiderscheit BC, Thelen DG, Enright T, Tuite MJ. MR observations of long-term musculotendon remodeling following a hamstring strain injury. Skeletal Radiology. 2008; 37:1101–1109. [PubMed: 18649077]

Silder A, Reeder SB, Thelen DG. The influence of prior hamstring injury on lengthening muscle tissue mechanics. Journal of Biomechanics. 2010; 43:2254–2260. [PubMed: 20472238]

Silder A, Westphal CJ, Thelen DG. A Magnetic Resonance-Compatible Loading Device for Dynamically Imaging Shortening and Lengthening Muscle Contraction Mechanics. Journal of Medical Devices. 2009; 3:1–5.

Spottiswoode BS, Zhong X, Hess AT, Kramer CM, Meintjes EM, Mayosi BA, Epstein FH. Tracking myocardial motion from cine DENSE images using spatiotemporal phase unwrapping and temporal fitting. IEEE Transactions on Medical Imaging. 2007; 26:15–30. [PubMed: 17243581]

Verrall GM, Slavotinek JP, Barnes PG, Fon GT. Diagnostic and prognostic value of clinical findings in 83 athletes with posterior thigh injury: Comparison of Clinical Findings with Magnetic Resonance Imaging Documentation of Hamstring Muscle Strain. The American Journal of Sports Medicine. 2003; 31:969–973. [PubMed: 14623665]

Woodley SJ, Mercer S. Hamstring muscles: architecture and innervation. Cells Tissues Organs. 2005; 179:125–141. [PubMed: 15947463]

Zajac FE. Muscle and tendon: properties, models, scaling, and application to biomechanics and motor control. Critical Reviews in Biomedical Engineering. 1989; 17:359–411. [PubMed: 2676342]

Zhong X, Epstein FH, Spottiswoode BS, Helm PA, Blemker SS. Imaging two-dimensional displacements and strains in skeletal muscle during joint motion by cine DENSE MR. Journal of Biomechanics. 2008; 41:532–540. [PubMed: 18177655]

Zhong X, Helm PA, Epstein FH. Balanced Multipoint Displacement Encoding for DENSE MRI. Magnetic Resonance in Medicine. 2009; 61:981–988. [PubMed: 19189288]

Zhong X, Spottiswoode BS, Meyer CH, Kramer CM, Epstein FH. Imaging three-dimensional myocardial mechanics using navigator-gated volumetric spiral cine DENSE MRI. Magnetic Resonance in Medicine. 2010; 64:1089–1097. [PubMed: 20574967]

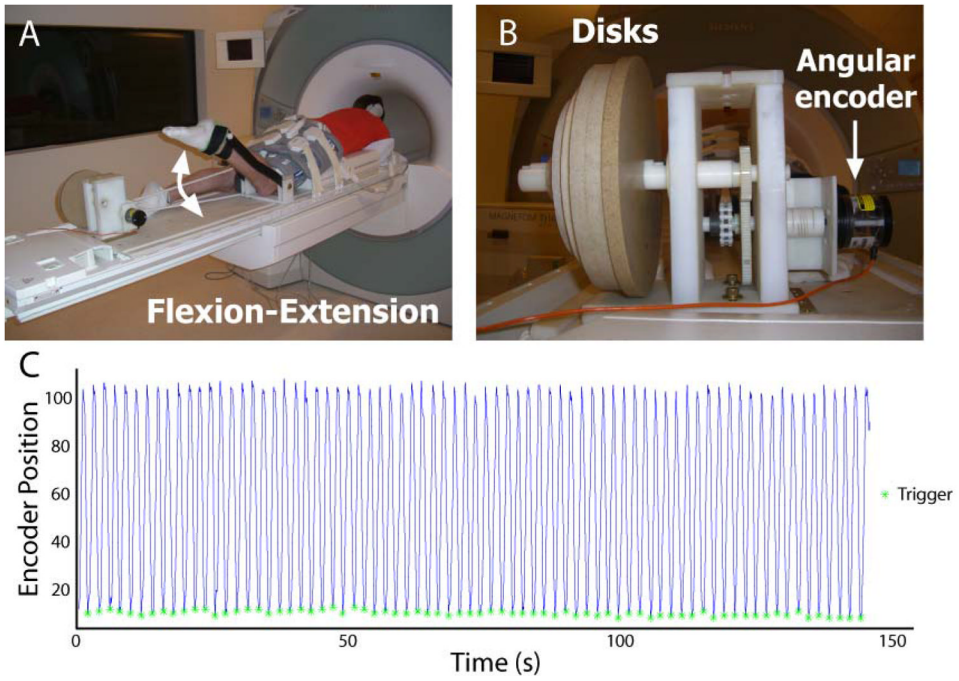

Figure 1. Experimental setup

Subjects were positioned in the head-first, prone position in an MR-compatible exercise device during repeated knee flexion and extension (subject pictured outside the scanner) (A). Cyclic rotation of inertial disks resulted in active lengthening of the biceps femoris muscle (Silder et al., 2009), while an angular encoder signal was sent to a laptop computer running LabVIEW (B). Encoder position values (line) were used to trigger the scanner (asterisk) to begin image acquisition at the onset of knee extension (C). (Example data are from a single DENSE acquisition.)

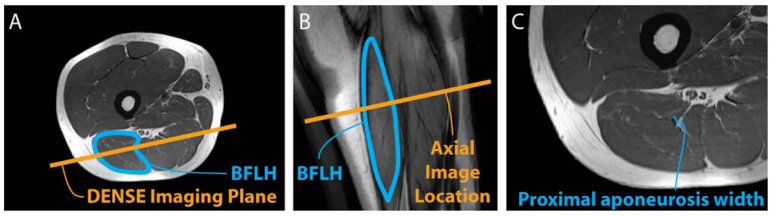

Figure 2. DENSE imaging plane and high-resolution images of the BFLH

The DENSE imaging plane was defined on axial plane high-resolution turbo spin-echo images (A), such that the plane included muscle tissue adjacent to the proximal aponeurosis of the BFLH muscle, the muscle belly, and the distal aponeurosis. Prior to DENSE image acquisition, a high-resolution image was obtained in the oblique-coronal DENSE imaging plane to verify the position of the BFLH and the inclusion of the aponeuroses (B). Proximal aponeurosis width measurements were taken directly on axial-plane images (C).

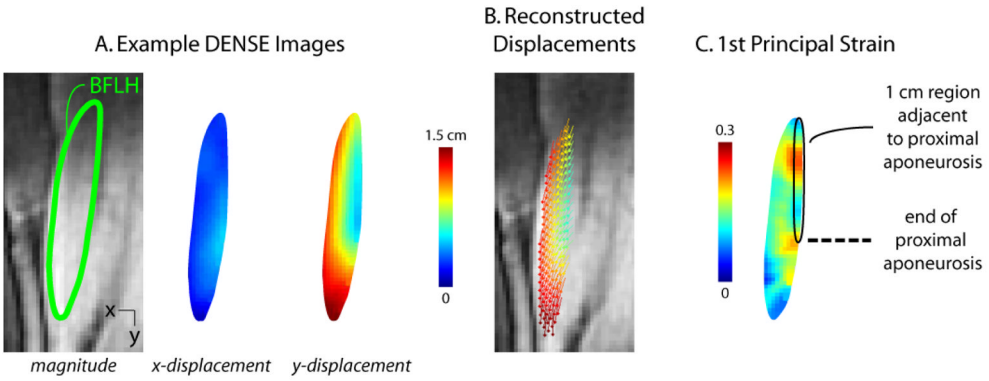

Figure 3. Example DENSE images, reconstructed displacements and strain map

Displacement encoding with stimulated echoes (DENSE) images were acquired in an oblique-coronal plane containing the biceps femoris long head muscle (A). Measured displacements were used to reconstruct time-varying tissue position at a pixel-wise resolution (B), where vectors represent displacement from the first image and the vector's color represents the magnitude of displacement. First principal strain was defined as the most positive eigenvalue of the Lagrangian strain tensor and was averaged in the region within approximately 1 cm of the proximal aponeurosis (C).

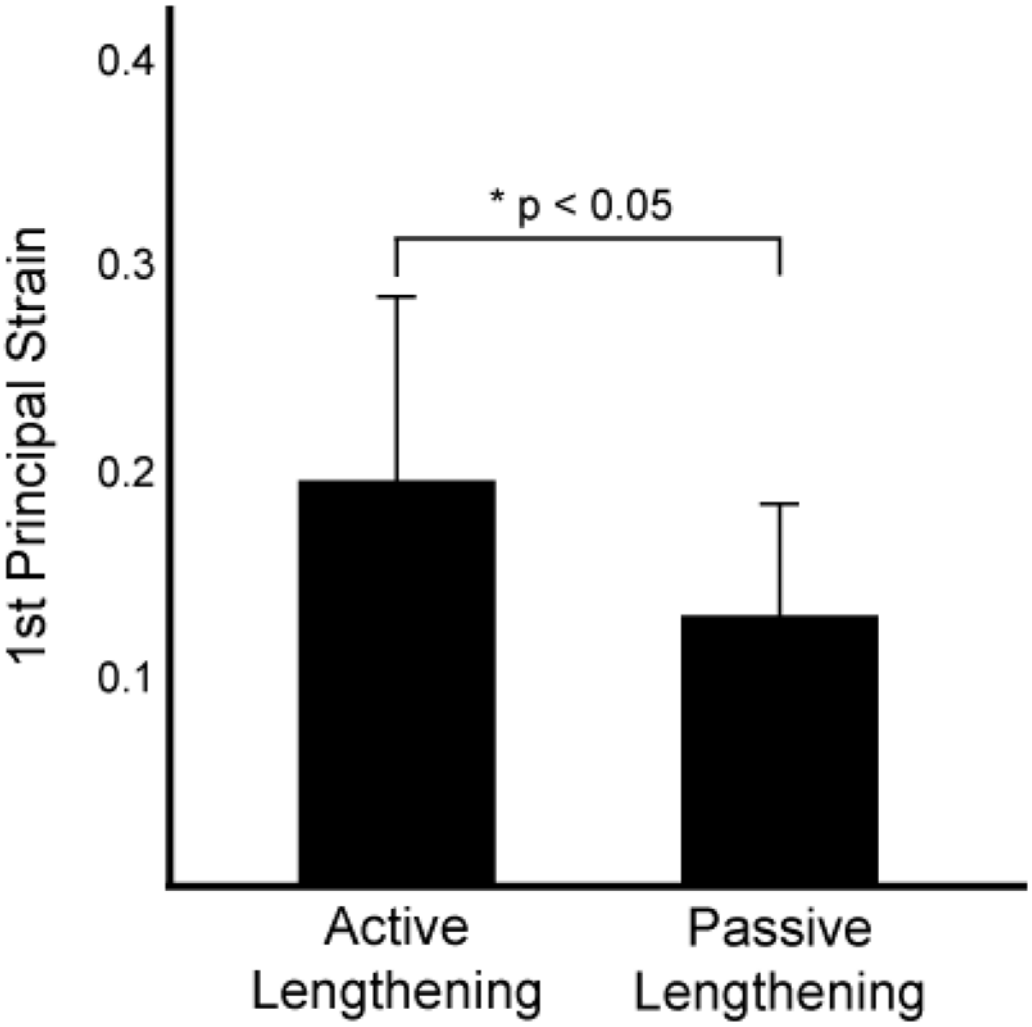

Figure 4. Activation strain results

Average 1st principal strain measurements in a region within approximately 1 cm of the proximal aponeurosis of the biceps femoris long head were significantly larger during active lengthening (0.19 SD 0.09) than passive lengthening (0.13 SD 0.06) (*p < 0.05).

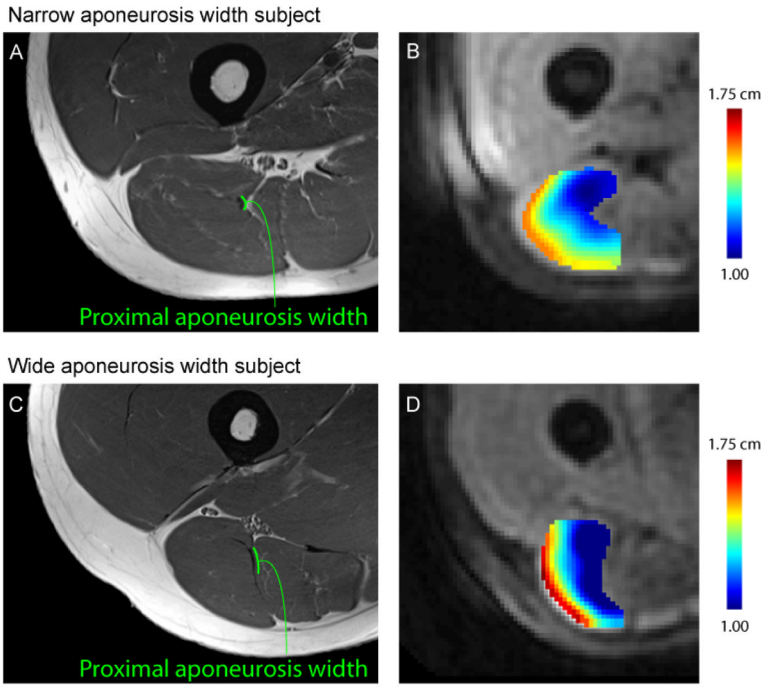

Figure 5. Example high-resolution images and displacement color maps

Example high-resolution image and aponeurosis width measurement for a representative subject with a narrow aponeurosis (A) and wide aponeurosis (C) during active lengthening. Color maps of displacement magnitude demonstrate a small region (i.e., area) of localized, low displacement adjacent to the proximal aponeurosis for a narrow width subject (B) relative to a wide aponeurosis width subject (D).

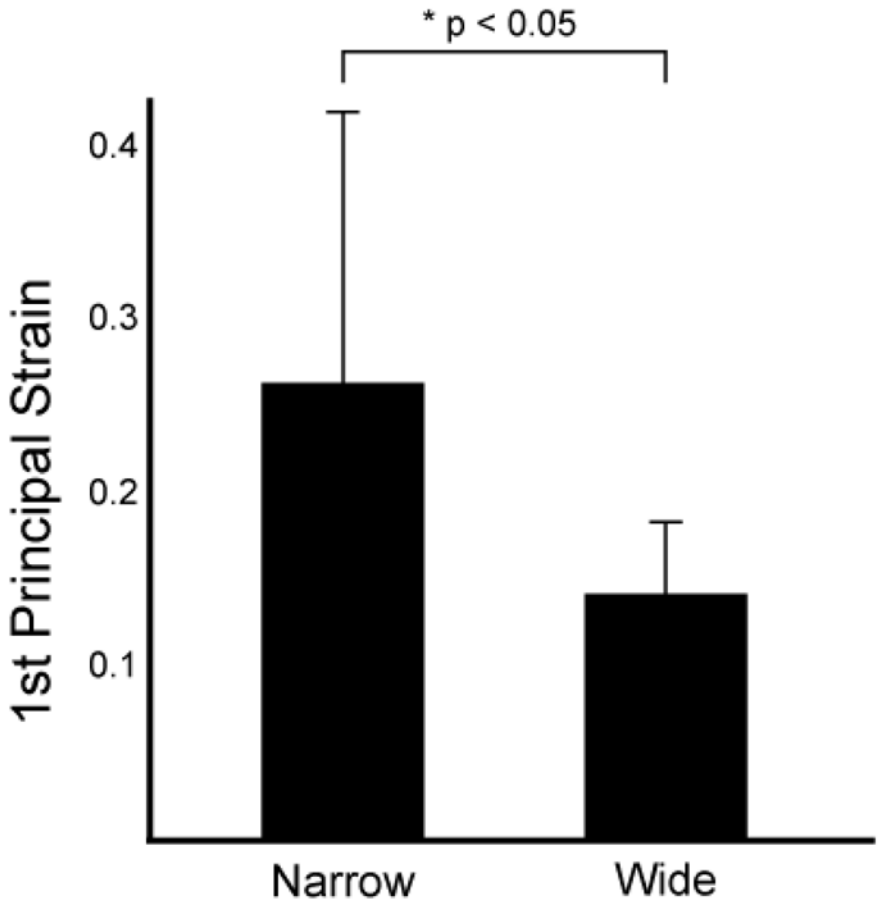

Figure 6. Aponeurosis width strain results

Average 1st principal strain measurements in a region within approximately 1 cm of the proximal aponeurosis of the biceps femoris long head were significantly larger for subjects with a narrow aponeurosis width (0.26 SD 0.15) than a wide aponeurosis width (0.14 SD 0.04) (*p < 0.05).